Classical and quantum chaos in the generalized parabolic lemon-shaped billiard

Lopac, Vjera; Mrkonjić, Ivana; Radić, Danko

Source / Izvornik: **Physical Review E, 1999, 59, 303 - 311**

Journal article, Published version
Rad u časopisu, Objavljena verzija rada (izdavačev PDF)

https://doi.org/10.1103/PhysRevE.59.303

Permanent link / Trajna poveznica: https://urn.nsk.hr/urn:nbn:hr:217:684999

Rights / Prava: In copyright / Zaštićeno autorskim pravom.

Download date / Datum preuzimanja: **2024-12-09**

Repository / Repozitorij:

Repository of the Faculty of Science - University of Zagreb

Classical and quantum chaos in the generalized parabolic lemon-shaped billiard

V. Lopac
Division of Physics, Faculty of Chemical Engineering and Technology, University of Zagreb, Zagreb, Croatia

I. Mrkonjić and D. Radić
Department of Physics, Faculty of Science, University of Zagreb, Zagreb, Croatia

(Received 4 June 1998)

Two-dimensional billiards of a generalized parabolic lemonlike shape are investigated classically and quantum mechanically depending on the shape parameter δ. Quantal spectra are analyzed by means of the nearest-neighbor spacing distribution method. Calculated results are well accounted for by the proposed new two-parameter distribution function $P(s)$, which is a generalization of Brody and Berry-Robnik distributions. Classically, Poincaré diagrams are shown and interpreted in terms of the lowest periodic orbits. For $\delta=2$, the billiard has some unique characteristics resulting from the focusing property of the parabolic mirror. Comparison of the classical and quantal results shows an accordance with the Bohigas, Giannoni, and Schmit conjecture and confirms the relevance of the new distribution for the analysis of realistic spectral data.
[S1063-651X(99)00401-8]

PACS number(s): 05.45.Mt, 03.65.−w

I. INTRODUCTION

One of the leading themes in the theory of quantum chaos is the connection between chaotic behavior in classical systems and statistical spectral properties of the corresponding quantal systems. Founding their investigations on statistical properties of nuclear and atomic spectra [1] and on results for two-dimensional quantum billiards obtained previously by Berry and Tabor [2], McDonald and Kaufmann [3], and Casati *et al.* [4], in 1984 Bohigas, Giannoni, and Schmit [5] expressed the conjecture (BGS) that quantal energy level spacings of ergodic systems whose classical counterparts exhibit chaotic behavior obey the Wigner [Gaussian orthogonal ensemble (GOE)] statistics, whereas for systems which are classically integrable the statistics is Poissonian. Although not rigorously proved, this conjecture has been confirmed by a number of examples. Possible exceptions have been discussed in different contexts [6–11]. The typical exception is the harmonic oscillator and other systems which are equivalent to it [2]. At present, it is generally accepted that the BGS conjecture expresses a generic property of quantal systems, in the sense of the definition of the word *generic* given by Berry [12]: there may be exceptions, but they form a set of measure zero.

A review of measured and calculated quantal level sequences in different domains of physics shows that for most systems the energy level statistics is intermediate between the two limits. In the nearest-neighbor spacing distribution (NNSD) method, reflecting the correlations in the quantal spectra, this transition is described by different distribution functions characterized by one or more control parameters [13–17].

In this paper we investigate, first quantum mechanically and then classically, a one-parameter family of two-dimensional billiards. We start with a lemon-shaped billiard defined by two parabolas, for which the shape parameter is $\delta=2$, and then distort it by introducing different values $\delta \neq 2$. This enables us to follow the change of statistics depending on the billiard shape.

Two-dimensional billiards belong among the oldest problems of quantum mechanics, but during the past two decades they have newly regained remarkable interest [12,18,19]. This is primarily due to the discovery that such simple systems, with only a few exceptions, exhibit chaotic behavior. Furthermore, the experiments in resonating cavities were performed with microwaves and acoustic waves [20–23]. In the quantal and semiclassical domain, the whole new field of mesoscopic physics developed from investigations of quantum dots, where only few electrons move almost classically in the ballistic regime within the billiardlike wells of micrometer dimensions [24,25].

The organization of the paper is as follows. In Sec. II we define the billiard shape and introduce the shape parameter δ. In Sec. III we solve the two-dimensional quantum-mechanical eigenvalue problem determined by the billiard boundary and obtain the energy level sequences. In Sec. IV, the calculated level densities are analyzed by means of the nearest-neighbor spacing distribution method. In Sec. V the same billiard is treated as a classical dynamical problem. The Poincaré plots are shown and the role of the lowest periodic orbits is briefly discussed. In Sec. VI, results from both quantum and classical analysis are reviewed, leading to conclusions on the applicability of the BGS conjecture and the proposed level density distributions.

II. DESCRIPTION OF THE GENERALIZED PARABOLIC LEMON-SHAPED BILLIARD

The generalized parabolic lemon-shaped billiard is defined in the x-y plane by the boundary

$$y(x)=\pm(1-|x|^{\delta}), \quad x\in[-1,1]. \tag{1}$$

For $\delta=2$, the boundary has a typical symmetrical lemon shape, defined by two parabolas. When the parameter δ is varied, the billiard shape changes, but remains within the square defined by diagonally opposed points $(-1,-1)$ and $(1,1)$ in the x-y plane (Fig. 1). We explore only the convex

 ©1999 The American Physical Society

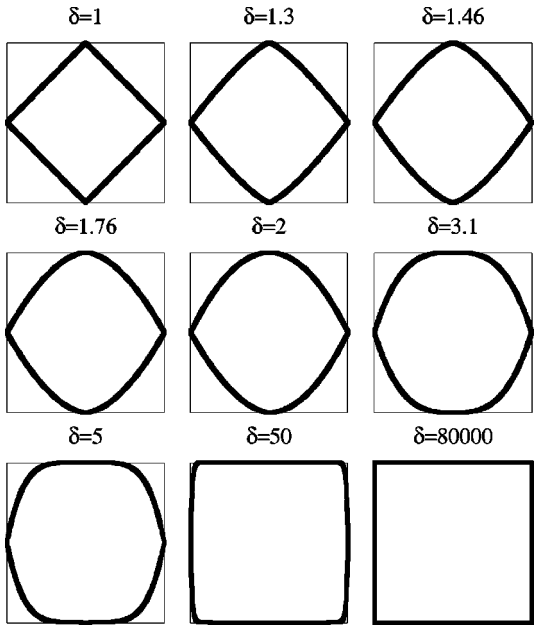

FIG. 1. Generalized parabolic lemonlike billiards for different values of the shape parameter δ.

boundaries in Eq. (1), thus $1 \leqslant \delta < \infty$. In the limit $\delta = 1$ one obtains the tilted square with the side $d = \sqrt{2}$. In the other limit $\delta \to \infty$, we have another square with $d = 2$. The parameter δ is closely related to the characteristic angle α of the billiard (1) (Fig. 2), since

$$\tan \frac{\alpha}{2} = \delta. \tag{2}$$

The Schrödinger equation is solved to obtain the wave functions and discrete energy levels, which is equivalent to finding stationary waves in the two-dimensional well with infinitely steep walls. In this paper we concentrate on the energy levels, and the discussion of the calculated wave functions will be given elsewhere [26].

The classical problem reduces to a particle of mass m within the billiard, bouncing elastically on the billiard walls and moving freely between the bounces. At each bounce the angle of incidence is equal to the reflection angle. Although the rules of motion are deterministic, the resulting dynamics can be regular, fully chaotic, or mixed, depending on the billiard shape.

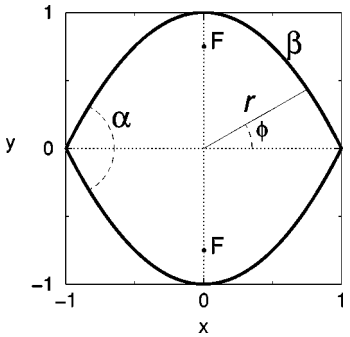

FIG. 2. Characteristics of the generalized parabolic lemonlike billiard described by the boundary $\beta \equiv \rho(\phi)$.

Proposing the parabolic billiard shape, we had several points in mind. First, among all planar curves, only the parabolic mirror has the unique property of reflecting parallely all rays passing through a certain focal point. Second, whereas the billiards shaped with the rectilinear, circular, elliptical, hyperbolic, and other interesting boundary segments [27–43] have already been explored, reports on the parabolic boundary shapes are practically nonexistent. Moreover, the distortion of the proposed shape by varying δ leads to a gradual transition between the two squares. It is interesting to see how this transition reflects itself in the classical and quantal properties.

Here we note that the transition from $\delta > 1$ to $\delta < 1$ introduces a dramatic change in the shape of the billiard (1). For $0 < \delta < 1$ the billiard boundary consists of four concave arcs, resulting in the shape and properties similar to those of the diamond billiard [5,27]. Therefore, this is a new class of billiards, which deserves special attention and will be treated separately.

III. THE QUANTUM-MECHANICAL BILLIARD PROBLEM

The Schrödinger equation for a particle of mass m moving freely within the billiard boundary in a two-dimensional billiard is identical to the Helmholtz equation

$$-\frac{\hbar^2}{2m}\nabla^2\Psi = E\Psi, \tag{3}$$

where E is the particle energy. The usual transformation to dimensionless variables is equivalent to substituting

$$\frac{\hbar^2}{2m} = 1 \quad \text{and} \quad E = k^2, \tag{4}$$

which yields

$$\left[\frac{\partial^2}{\partial x^2} + \frac{\partial^2}{\partial y^2} + k^2\right]\Psi(x,y) = 0. \tag{5}$$

In polar coordinates (Fig. 2), Eq. (5) becomes

$$\left[\frac{\partial^2}{\partial r^2} + \frac{1}{r}\frac{\partial}{\partial r} + \frac{1}{r^2}\frac{\partial^2}{\partial \phi^2} + k^2\right]\Psi(r,\phi) = 0. \tag{6}$$

After the separation of variables, one obtains the factorized wave function

$$\Psi(r,\phi) = R(r)\Phi(\phi). \tag{7}$$

Solutions can be classified according to symmetry. The twofold reflection symmetry (on the x and y axis) of the original billiard causes degeneracies, which we avoid in our calculations by taking only the even-even solutions, i.e., those which obey the condition $\Psi(x,y) = \Psi(-x,y) = \Psi(x,-y)$. We are then left with the wave function in the form

$$\Psi(r,\phi) = \sum_{\nu=2,4,6,\ldots}^{\infty} [B_\nu \cos(\nu\phi)] J_\nu(kr), \tag{8}$$

where the sum is over the even integer values of ν, and $J_\nu(kr)$ is the Bessel function of the first kind with index ν.

To compute the energies of stationary states and coefficients in the wave functions, we have written the program based on the method introduced by Ridell [44]. We limit our calculation to a finite energy interval, which enables us to stop the summation in Eq. (8) at the certain Nth energy level. The Dirichlet boundary condition

$$\Psi(\mathbf{r})|_{\mathbf{r}=\beta}=0, \tag{9}$$

with $\beta\equiv\rho(\phi)$ (Fig. 2), is assured for N points on the boundary curve having coordinates ϕ_i and $\rho(\phi_i)$. This results in a system of N linear equations, whose solution is nontrivial only if

$$\det|\cos(i\phi_j)\cdot J_i(k\rho(\phi_j))|=0. \tag{10}$$

Here i takes on the values of first N even integers, j are the integers between 1 and N, and ϕ_j are N angles chosen between 0 and $\pi/2$. Equation (10) gives the values of k determining the energies (4). In our calculation the values of k were limited to the interval $k\in[0,150]$, the step in searching for k was 0.01 or smaller, the precision was 10^{-8}, and, depending on the value of δ, between 900 and 1500 states were obtained.

IV. ENERGY LEVEL STATISTICS FOR THE GENERALIZED PARABOLIC LEMON-SHAPED BILLIARD

The level sequences obtained in the quantal calculation were unfolded following the prescription of French and Wong [45] and then analyzed by fitting to the theoretical distribution functions $P(s)$. Related to $P(s)$ are the cumulative distribution $W(s)=\int_0^s P(\sigma)d\sigma$ and the gap distribution $Z(s)=\int_s^\infty d\sigma(\sigma-s)P(\sigma)$. The gap distribution is the probability that no level spacing is present in the interval between s and $s+\Delta s$. Relation between the level spacing distribution $P(s)$ and the gap distribution is $P(s)=d^2Z(s)/ds^2$. Three types of theoretical distributions were used to account for transition between the two limiting cases, the Poissonian level density distribution

$$P^{\mathrm{P}}(s)=e^{-s} \tag{11}$$

and the Wigner distribution

$$P^{\mathrm{W}}(s)=\frac{\pi}{2}se^{-(\pi/4)s^2}. \tag{12}$$

First is the Brody distribution [46], depending on the parameter ω and given as

$$P^{\mathrm{B}}(s)=\alpha(\omega+1)s^\omega e^{-\alpha s^{\omega+1}} \tag{13}$$

with

$$\alpha=\left[\Gamma\left(\frac{\omega+2}{\omega+1}\right)\right]^{\omega+1}. \tag{14}$$

This distribution is identical to Poisson for $\omega=0$ and to Wigner for $\omega=1$. There is no exact derivation which would explain the physical meaning of ω, but there are strong indications supporting the idea that the parameter ω reflects the degree of the level repulsion within a spectral sequence. Since ω is an empirical parameter, it can be allowed to take on all the values $-1<\omega\leqslant 1$, the negative values being appropriate if for small spacings the calculated distribution is steeper than the Poisson curve.

The other well known distribution is that of Berry and Robnik [47]. It is characterized by the parameter q and reads

$$P^{\mathrm{BR}}(s)=e^{(q-1)s}\left[(1-q)^2\mathrm{erfc}\left(\frac{\sqrt{\pi}}{2}qs\right)\right]+\left(2q(1-q)+\frac{\pi}{2}q^3s\right)e^{-(\pi/4)q^2s^2}. \tag{15}$$

The error function is defined as

$$\mathrm{erfc}(x)=\frac{2}{\sqrt{\pi}}\int_x^\infty e^{-t^2}dt. \tag{16}$$

This distribution coincides with Wigner for $q=1$ and with Poisson for $q=0$. The two distributions are conspicuously different in the fact that the probability of very small spacings vanishes in the Brody distribution for all values of ω, whereas in the Berry-Robnik distribution it is $P^{\mathrm{BR}}(0)=1-q^2$. Besides, the Berry-Robnik parameter q has a well defined physical meaning: quantitatively it is the fraction of the phase space which is filled with chaotic trajectories, whereas the remaining regular fraction of the phase space is equal to $1-q$. However, the Berry-Robnik distribution is exactly applicable only in the semiclassical limit, and we are exploring the complete spectrum, including the lowest-lying levels.

The third theoretical distribution we apply in our analysis is the two-parameter function introduced by Lopac [48] and Lopac, Brant, and Paar [49]. In [49], applied to nuclear model spectra, it approximated the calculated histograms better than Brody or Berry-Robnik distributions. This new distribution is a generalization of both Brody and Berry-Robnik distributions, and has two parameters, ω and q. It reads

$$P(s)=e^{-(1-q)s}(1-q)^2Q\left[\frac{1}{\omega+1},\alpha q^{\omega+1}s^{\omega+1}\right]+e^{-(1-q)s}q[2(1-q)+\alpha(\omega+1)q^{\omega+1}s^\omega]\times e^{-\alpha q^{\omega+1}s^{\omega+1}}. \tag{17}$$

Here, α is defined as in Eq. (14) and Q denotes the incomplete Γ function,

$$Q(a,x)=\frac{1}{\Gamma(a)}\int_x^\infty e^{-t}t^{a-1}dt. \tag{18}$$

The derivation of Eq. (17) was based on the factorized gap distribution $Z^{\mathrm{PR}}(s)$,

$$Z^{\mathrm{PR}}(s)=e^{-(1-q)s}Q\left[\frac{1}{\omega+1},\alpha q^{\omega+1}s^{\omega+1}\right], \tag{19}$$

introduced by Prosen and Robnik [50]. They applied the distribution (19) (named in [50] the Berry-Robnik-Brody distri-

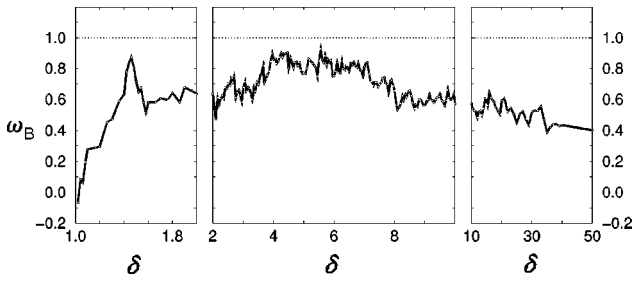

FIG. 3. Values of the Brody parameter ω_B in Eq. (13), obtained in the NNSD analysis of the quantal billiard spectra, in dependence on the shape parameter δ. Horizontal dotted lines (lower and upper) denote the regular and chaotic limits, respectively.

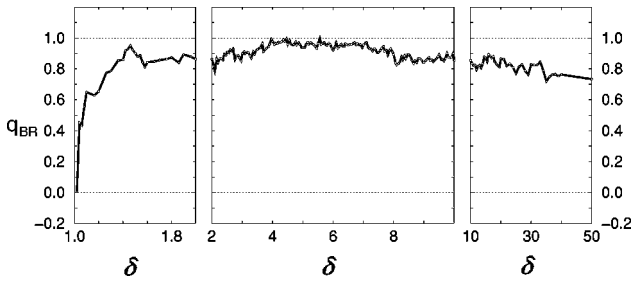

FIG. 4. Values of the Berry-Robnik parameter q_{BR} in Eq. (15), obtained in the NNSD analysis of the quantal billiard spectra, in dependence on the shape parameter δ. Horizontal dotted lines (lower and upper) denote the regular and chaotic limits, respectively.

bution) to the Robnik billiard [33,34] and obtained a very good agreement. Their conclusion implies that the distribution (17) describes simultaneously the transition from the semiclassical to the quantal regime and the transition from integrability to chaos. The two parameters ω and q characterize these two transitions, respectively, so that q retains its meaning as the chaotic fraction of the phase space. In this case, however, it is applicable also to cases far from the semiclassical limit. The parameter ω describes the degree of level repulsion in the given spectral sequence and is essentially connected with the localization of the underlying chaotic states [51].

It should be stressed that the distribution (17) is a generalization of both Eqs. (13) and (15). It is identical with Brody (13) when $q=1$ and with Berry-Robnik (15) when $\omega=1$. With $q=0$ one obtains the Poisson distribution (11) for all values of ω, and if simultaneously $\omega=1$ and $q=1$, the result is the Wigner (GOE) distribution (12). Graphical representation of Eq. (17) in dependence on ω and q is given in [49].

The analysis of calculated results shows that the fitting parameters of all three distributions follow the same trend when the system control parameter is varied. However, all computations in which the distributions (17) or (19) were applied so far, show that these distribution functions give a better fit than the Brody or Berry-Robnik distributions.

In the present paper our main interest is to explore the dependence of the values ω and q for the three proposed distributions on the parameter δ characterizing the shape of the billiard. In the following, we shall use symbols ω_B and q_{BR} to denote the Brody and Berry-Robnik parameters, respectively, and ω and q for the parameters of the distribution (17). Results are shown in Fig. 3 for Brody distribution, in Fig. 4 for Berry-Robnik distribution, and in Fig. 5 for the generalized distribution (17).

Figure 3 shows results of the fitting of the calculated level spacing histogram to the Brody distribution. One observes a gradual transition from slightly negative values to a sharp local maximum at $\delta=1.46$ with $\omega_B=0.876$. There is also a minimum of $\omega_B=0.513$ at $\delta=1.58$, followed by a slow and oscillating growth, with another minimum slightly above the value of $\delta=2$. The maximal value is $\omega_B=0.928$ at $\delta=5.56$. In the interval $4\leqslant\delta\leqslant7$, ω_B is greater than 0.7, which, in BGS and Brody terms, means a high degree of chaoticity. The oscillations are sharp and very sensitive to the shape variation. A minimal change in shape can induce dramatic changes in the degree of chaotic behavior. The reason for this is clearer when one explores the occurrence and disappearance of certain classical orbits (see Sec. V). Furthermore, by changing δ, the angle α in Eq. (2) is varied. Investigations of triangular and rhomboid billiards (which in certain features resemble our system) have shown that the incommensurability with π of the billiard angle is a decisive property determining the billiard dynamics [36].

Results for Berry-Robnik distribution shown in Fig. 4 fully confirm the discussion of Fig. 3, except that the values of q_{BR} are shifted upwards in comparison with ω_B. Otherwise, the positions of local maxima and minima are exactly the same. As in Fig. 3, for large δ a slow but steady decrease of q_{BR} is observed, leading to the zero values for $\delta\to\infty$. Since the calculation of quantal spectra in our method becomes computationally very sensitive for nearly quadratic shapes (when $\delta\to\infty$), we show our results only for $\delta\leqslant50$.

In applying the generalized distribution (17) to the billiard (1), we hold both parameters ω and q within the limits [0,1]. Results are shown in Fig. 5(a) for ω and in Fig. 5(b) for q. For most δ the value of ω oscillates around $\omega=0.7$. For $\delta\leqslant2$, the oscillations are more conspicuous and have larger deviations. For large δ, the values of ω become slightly

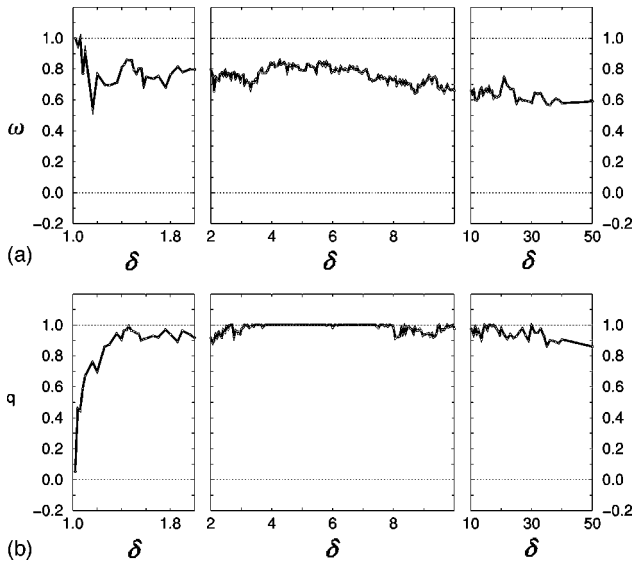

FIG. 5. Values of the parameters ω (a) and q (b) of the two-parameter distribution (17), obtained in the NNSD analysis of the quantal billiard spectra, in dependence on the shape parameter δ. Horizontal dotted lines (lower and upper) denote the regular and chaotic limits, respectively.

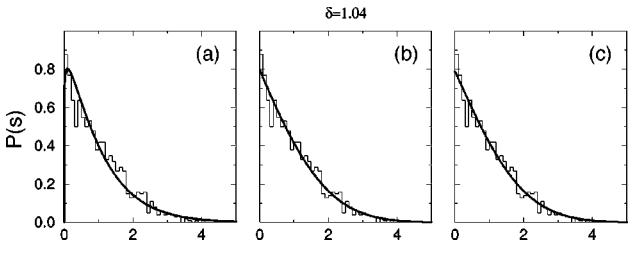

FIG. 6. (a) Brody distribution (13), (b) Berry-Robnik distribution (15), and (c) the two-parameter distribution (17) (full line) fitted to the calculated $P(s)$ (histogram) for $\delta=1.04$. Values obtained in the fitting procedure are $\omega_B=0.081$, $q_{BR}=0.450$, $\omega=0.948$, and $q=0.460$.

smaller. The results reflecting the degree of chaoticity in the sense of the BGS conjecture are given by the value of q, and are shown in Fig. 5(b). The total interval of δ can be divided into several regions. First is one with δ between 1 and 1.46, where q grows from 0 to 1 and depicts the transformation of the quadratic shape into more complicated lemonlike forms. Approximately in the intervals $1.46\leqslant\delta\leqslant4$ and $7\leqslant\delta\leqslant30$, the value of q oscillates around 0.9, whereas it is equal to 1 practically everywhere in the central interval between $\delta=4$ and $\delta=7$. For very large δ, results of our calculations indicate the slow decrease towards the limiting result $q=0$.

From results obtained and shown in Figs. 3, 4, and 5, we conclude that the transition of the shape from the square with the side equal to $\sqrt{2}$ via different lemonlike shapes to another square (with the side equal to 2) is accompanied by the transition from the Poisson to the Wigner (GOE) statistics and again to the Poisson. In the central region there is a highly developed chaos, and in the neighboring intervals the measures of chaos show an oscillatory transitional behavior.

To illustrate the applicability of the intermediate distributions (13), (15), and (17) for quantifying these transitions, we show the histograms and the fitted theoretical distributions for $\delta=1.04$ (Fig. 6), $\delta=2$ (Fig. 7), and $\delta=5$ (Fig. 8). Figures 6–8 enable us to compare the three theoretical curves and their ability to describe realistic histograms. The crucial criterion should be the agreement at small spacings $s\approx0$ and applicability to the complete spectrum. The distribution (17) satisfies all these conditions. The inspection of the corresponding cumulative transition distributions [49,50], which are valuable because they do not depend on the bin width, further confirms that the value of q of the generalized distribution (17) is the key result of the statistical level density investigation, suitable for discussions in the context of the BGS conjecture.

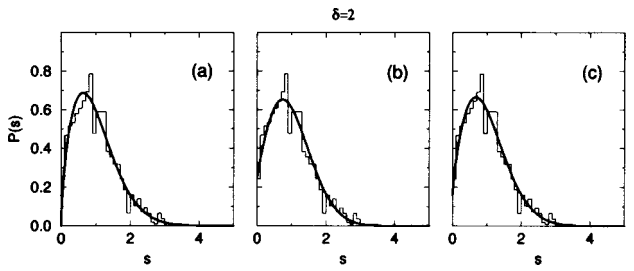

FIG. 7. (a) Brody distribution (13), (b) Berry-Robnik distribution (15), and (c) the two-parameter distribution (17) (full line) fitted to the calculated $P(s)$ (histogram) for $\delta=2$. Values obtained in the fitting procedure are $\omega_B=0.638$, $q_{BR}=0.863$, $\omega=0.796$, and $q=0.916$.

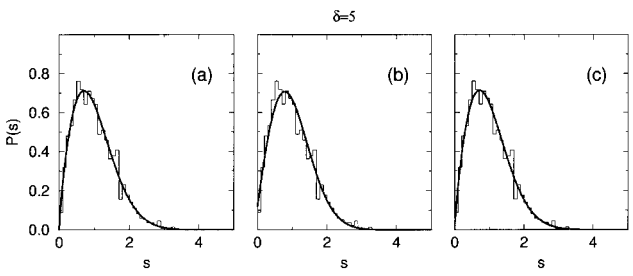

FIG. 8. (a) Brody distribution (13), (b) Berry-Robnik distribution (15), and (c) the two-parameter distribution (17) (full line) fitted to the calculated $P(s)$ (histogram) for $\delta=5$. Values obtained in the fitting procedure are $\omega_B=0.775$, $q_{BR}=0.938$, $\omega=0.791$, and $q=1.000$.

At this point it should be said that our analysis of the obtained level sequences included also the Δ_3 statistical method [5,49], revealing the long-range correlations within the quantal spectrum. To compare the results of the two methods, we choose the value of $\Delta_3(5)$ as a convenient measure of the degree of chaoticity, and plot it in dependence on the shape parameter δ. The results are shown in Fig. 9. The comparison of Fig. 9 with Figs. 3–5 shows that the Δ_3 results, both globally and locally, reproduce the behavior obtained with the nearest-neighbor spacing distribution method. A more detailed Δ_3 analysis is now being performed in connection with the billiard wave functions and will be reported elsewhere [26].

V. PROPERTIES OF THE CLASSICAL GENERALIZED PARABOLIC LEMON-SHAPED BILLIARD

In analyzing properties of classical billiards, we concentrate our attention on the Poincaré sections for given δ and identify the contributing periodic trajectories. We limit our calculations to the first quadrant, i.e., to the quarter of the total billiard area. The procedure is as follows: for a given billiard we choose some initial data for positions x and y and velocity components v_x and v_y. We then calculate the position and velocity components at each of the successive collisions with the billiard wall. Typical calculations include 2×10^4 to 2×10^5 successive impacts. The results obtained

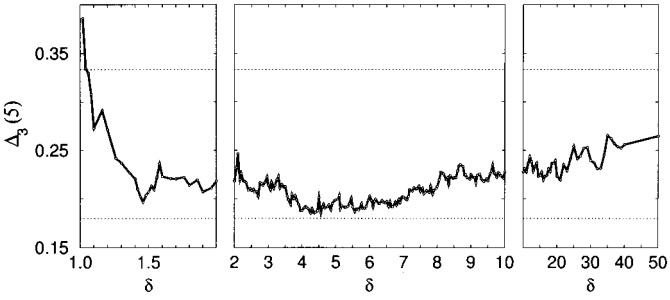

FIG. 9. Values of $\Delta_3(5)$, obtained in the spectral rigidity calculation for the quantal billiard spectra, in dependence on the shape parameter δ. Horizontal dotted lines (lower and upper) denote the chaotic and regular limits, respectively.

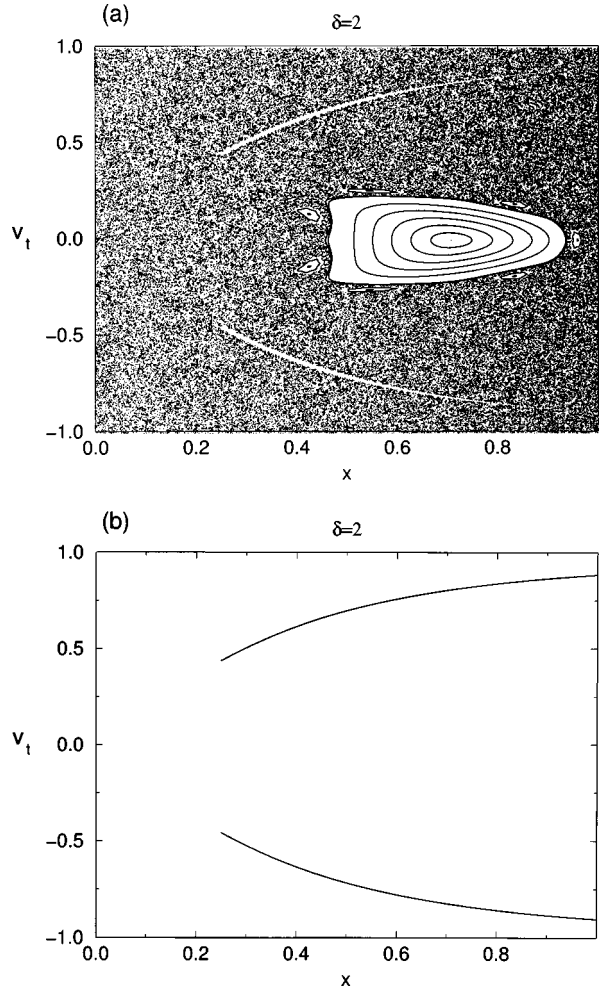

FIG. 10. (a) Poincaré plot for the parabolic billiard ($\delta=2$), obtained with conveniently selected sets of initial values. (b) Poincaré plot for the parabolic billiard ($\delta=2$), obtained with initial values $x_0=0$, $y_0=0.75002$, and $v_{y,0}/v_{x,0}=0.74999$. Practically the same picture is obtained by plotting all invariant points $(x, v_t = \pm 2x/\sqrt{1+4x^2})$ with $0.25<x<1$.

are plotted in the form of Poincaré diagrams. The horizontal axis shows the position x of the impact point, since the length of the arc variable [29] is much less suitable here than in the billiards having circular walls. On the vertical axis we plot the tangential component v_t of the velocity with respect to the billiard boundary, with the absolute value of the velocity $|v|=1$.

A. Classical dynamics of the parabolic lemon-shaped billiard ($\delta=2$)

Poincaré diagrams for the parabolic lemon-shaped billiard $\delta=2$ are shown in Fig. 10. In Fig. 10(a) the main regular area is observed, centered around the invariant point which originates in the trajectory of period 2, shown in Fig. 11(a). This trajectory passes through the origin and hits the boundary at the point $(x=1/\sqrt{2},\ y=1/2)$. For slight deviations of these initial conditions, the KAM theorem is valid, corresponding to trajectories shown in Fig. 11(b). The elliptical island resulting from this motion is surrounded by a boundary layer of great complexity [52]. Within this boundary the most conspicuous is the structure containing seven islands,

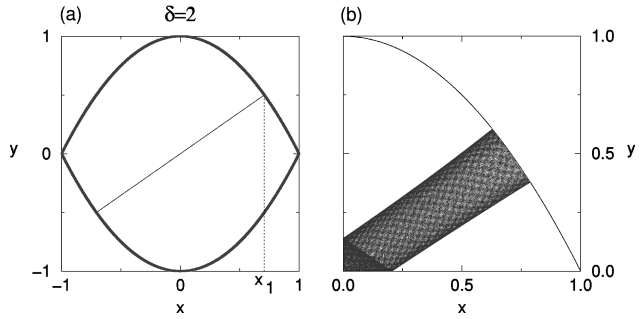

FIG. 11. The periodic orbit of period 2 for the whole billiard (a) and its surrounding KAM orbits for the quarter of the parabolic billiard for $\delta=2$ (b), calculated with the initial conditions $x_0=0.2$, $y_0=0$, and $v_{y,0}/v_{x,0}=0.7$. This orbit is responsible for the large regular region in Fig. 10(a).

whose origin is in the trajectory of period 14, shown in Fig. 12, and whose rich structure is revealed when a part of Fig. 10(a) is enlarged (Fig. 13). The KAM trajectories corresponding to it are also shown in Fig. 12. After exhibiting more and more complicated fractal structure, a small variation of the initial conditions is sufficient for the diffusion to take place. The motion becomes chaotic, and the trajectory fills almost the entire phase plane.

As there exists another trajectory of period 2, that which is spanned between the two opposite points on the vertical axis, one would expect another regular area. However, this is an isolated orbit, extremely unstable with respect to small variations of initial conditions, and in Fig. 10(a) it is reduced to two points completely immersed in the chaotic sea.

In Fig. 10(a), however, another regular area is observed, having the shape of two narrow arcs. The origin of this narrow region of regularity is the special focusing property of the parabolic mirror, namely that all rays, passing through the focal point, after reflection are parallel to each other. In the present case, the focal points are $(x_F=0,\ y_F=\pm\frac{3}{4})$ (Fig. 2). There is an infinite number of such trajectories of period 4, and they have the quadrangular, trapeze shape (Fig. 14). Vertical segments of such a trajectory intersect the horizontal axis in points x_1 and x_2, obeying the condition

$$4x_1x_2+1=0. \tag{20}$$

The tangential velocity components v_t corresponding to the position x_1 obey the equation

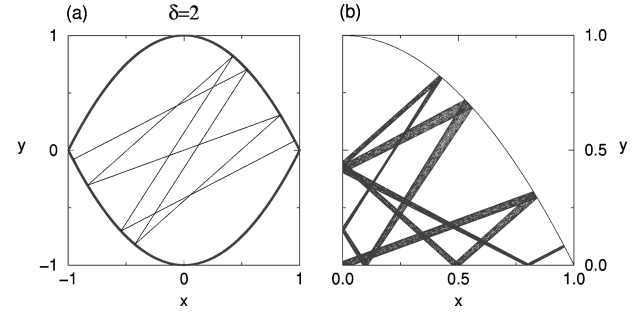

FIG. 12. The periodic orbit of period 14 for the whole billiard (a) and its surrounding KAM orbits for the quarter of the parabolic billiard for $\delta=2$ (b), calculated with the initial conditions $x_0=0.5$, $y_0=0$, and $v_{y,0}/v_{x,0}=0.9$. This orbit is responsible for seven small regular islands in Fig. 10(a).

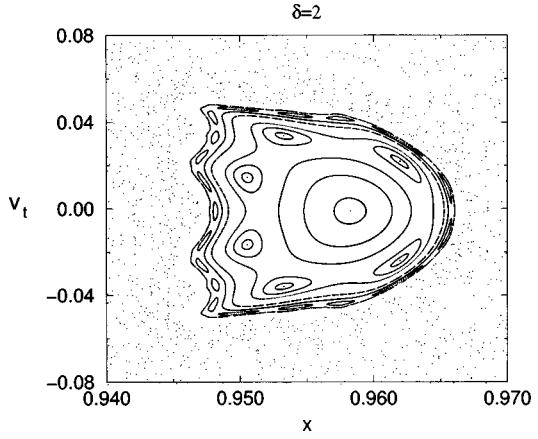

FIG. 13. Enlarged picture of one of the seven small islands in Fig. 10(a), having their origin in the periodic orbit shown in Fig. 12.

$$2x_1 \pm v_t\sqrt{1+4x_1^2}=0, \tag{21}$$

so that the two continuous lines, consisting of invariant points (x_1,v_t), extend between the end points $(1/4,\pm 1/\sqrt{5})$ and $(1,\pm 2/\sqrt{5})$. The $\pm$ signs are for positive and negative branch, respectively, corresponding to two possible directions of motion on each trajectory. Among all these trajectories we point out two which are of special interest: first, the rectangular one for $x_1=-x_2=1/2$, and second, the limit $x_1=1/4$ defining a ray-splitting situation, which asymptotically tends to a trajectory of period 3 (Fig. 15). This limiting case, however, is never realized, because of the sharp billiard angle (Fig. 2). On the Poincaré diagram points defined by Eqs. (20) and (21) describe a continuous curve. However, virtually the same picture, a flight of points, is obtained for a single choice of initial parameters, if some of the initial conditions leading to regular behavior are slightly distorted [Fig. 10(b)].

The described trajectories of period 4 are rather unstable. They are not surrounded by elliptic invariant curves, and therefore do not introduce much regularity into the problem. A closer inspection, requesting an extremely fine parameter regulation, would reveal the starlike structures in the small area surrounding each of the points, such as those described in [52].

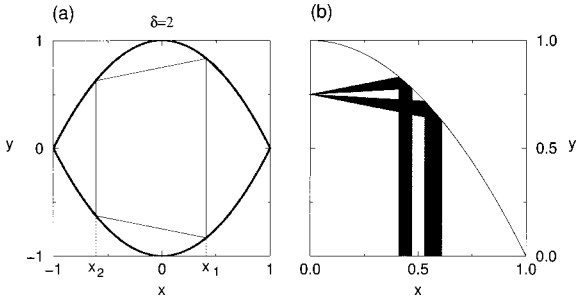

FIG. 14. Periodic orbit of period 4 for the whole billiard (a) and its surrounding KAM orbits for the quarter of the parabolic billiard for $\delta=2$ (b), calculated with the initial conditions $x_0=0$, $y_0=0.75005$, and $v_{y,0}/v_{x,0}=0.2$. These orbits are responsible for the two narrow arcs in Fig. 10(a) and two continuous curves on Fig. 10(b).

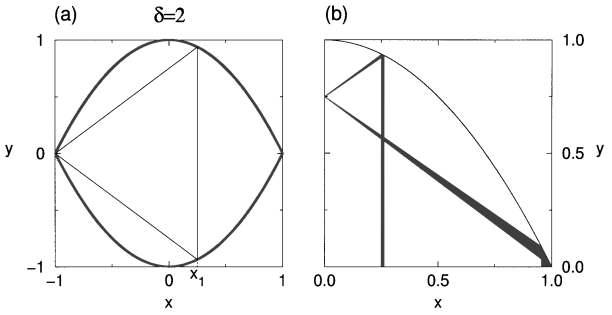

FIG. 15. (a) The ray-splitting limit of the quadrangular orbit shown in Fig. 14; (b) The corresponding KAM orbits obtained with the initial conditions $x_0=0$, $y_0=0.750\,001$ and $v_{y,0}/v_{x,0}=0.75$.

The Poincaré plots and the analysis of trajectories of lowest periods lead to the conclusion that the classical dynamics of the billiard (1) with $\delta=2$ is mixed and that the situation is close to the chaotic limit.

B. Classical dynamics in the billiards with $\delta\neq 2$

Here we investigate the effects of the shape variation on the Poincaré plots for $\delta\neq 2$. In order to compare classical and

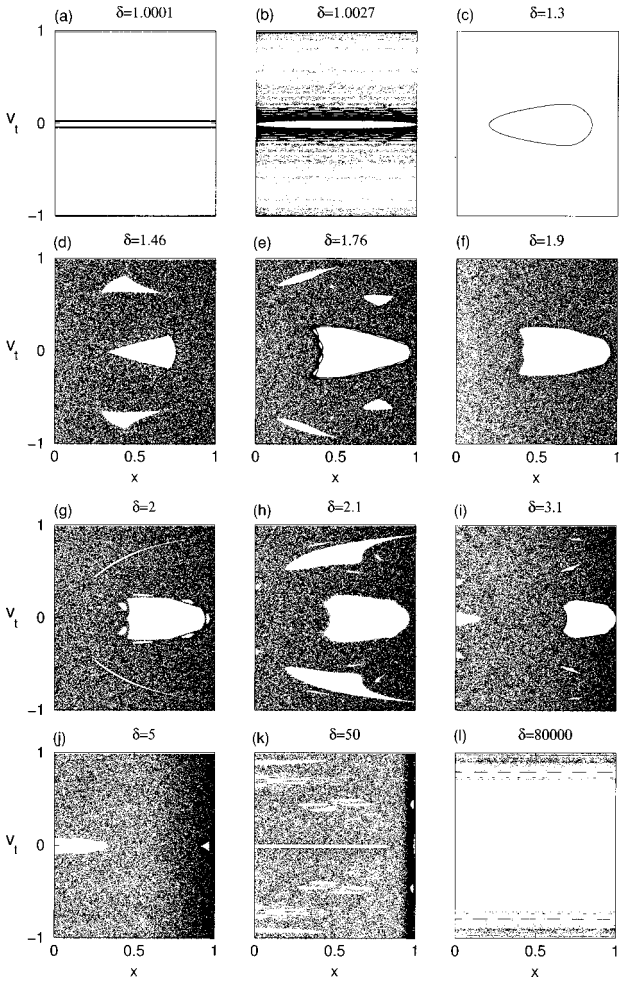

FIG. 16. Poincaré plots for generalized parabolic lemonlike billiards with (a) $\delta=1.0001$; (b) $\delta=1.0027$; (c) $\delta=1.3$; (d) $\delta=1.46$; (e) $\delta=1.76$; (f) $\delta=1.9$; (g) $\delta=2$; (h) $\delta=2.1$; (i) $\delta=3.1$; (j) $\delta=5$; (k) $\delta=50$, and (l) $\delta=80\,000$, obtained with the initial conditions $x_0=0.6$, $y_0=0$, and $v_{y,0}/v_{x,0}=0.925$.

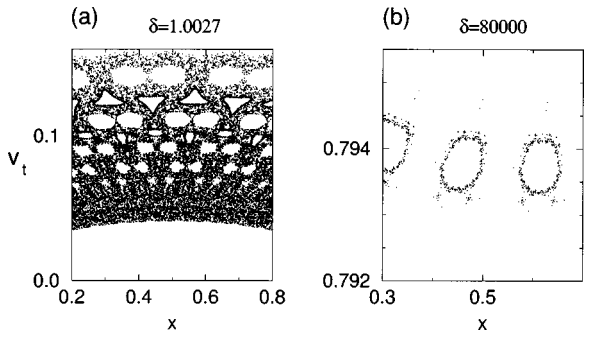

FIG. 17. Enlarged parts of the Poincaré plots shown in Fig. 16 for (a) $\delta=1.0027$ and (b) $\delta=80\,000$.

quantum results, we show Poincaré diagrams for a single set of initial conditions and for some chosen values of δ (Fig. 16). We first point out the Poincaré plots for δ close to the two limiting squares. The motion is nearly regular, and the straight lines obtained would degenerate into a web of points in the extreme limits of $\delta=1$ and $\delta\to\infty$. The apparently simple picture, however, on closer inspection reveals a rich fractal structure before the integrability is established, as shown in Fig. 17 by enlarging parts of Fig. 16 for $\delta=1.0027$ and $\delta=80\,000$.

In the general case, besides the isolated orbit along the vertical diameter of the billiard, trajectories of period 2 (Fig. 11) exist for all δ. The values of corresponding x_1 are obtained by solving the equation

$$\delta(1-x^{\delta})x^{\delta-2}-1=0. \tag{22}$$

For $1<\delta\leqslant 2$ there is only one solution, and for $\delta>2$ there are two solutions. Figure 18 shows the corresponding positions x_1 in dependence on δ, illustrating the creation of new periodic orbits when the billiard shape changes.

As for trajectories of higher degrees, it is easy to show that there is no triangular trajectory, regardless of the value of δ. For $\delta\neq 2$ the picture obtained for $\delta=2$ is changed. Of the trapezoidal trajectories of period 4 only the rectangular one survives. Figure 16 shows how a new elliptical regular region emerges from the point when δ changes from 2 to 2.1. For an arbitrary δ, the value of x_1 in Fig. 14 is found by solving the equation

$$\delta x^{\delta-1}-1=0. \tag{23}$$

It is possible that for some values of δ certain special higher-order regular trajectories occur, but these are sensitive to the small shape variations. The result is the so-called ''breathing chaos'' already observed in other billiard types [29].

The Poincaré plots for intermediate values of δ confirm the presence of chaos in the central zone between $\delta=4$ and $\delta=7$.

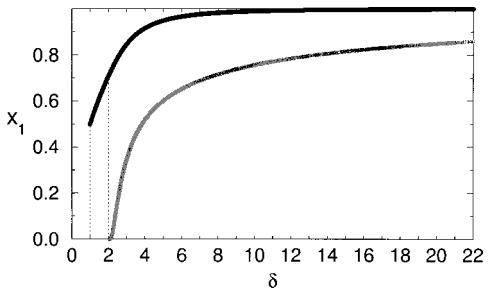

FIG. 18. Values of x_1 for periodic orbits of period 2, of the type shown in Fig. 11, for the generalized parabolic lemon-shaped billiards. There is only one such orbit for $1<\delta<2$, but there are two of them for $2\leqslant\delta<\infty$. Both values of x_1 approach 1 when $\delta\to\infty$.

VI. DISCUSSION AND CONCLUSIONS

In this work we have explored the classical and quantal dynamics of the generalized parabolic lemon-shaped billiards. First we calculated the energy level sequences for a large set of possible shape parameter values δ. Then we performed statistical analysis of the spectral densities using three different distribution functions $P(s)$. Finally we examined the possible periodic trajectories of the lowest order in corresponding classical billiards and presented the Poincaré diagrams for some chosen values of δ.

In conclusion, we state that the parabolic billiard has some interesting features, due to the reflection properties of the parabolic mirror, shown in the corresponding Poincaré diagrams. In spite of a large number of periodic trajectories, only a few of them are of elliptical (KAM) type, and therefore the dynamics is closer to the chaotic limit. The billiards with $\delta\neq 2$ exhibit a transition from quasiregular behavior near $\delta=1$ and when $\delta\to\infty$, and are chaotic in the central region between $\delta=4$ and $\delta=7$. In other regions the behavior is mixed.

Comparison of classical results and the results of the nearest-neighbor spacing distribution method for quantal energy level densities shows that, within the limits set by the applied computational method, the classical behavior and quantal results are in agreement, and that the present example gives another confirmation of the BGS conjecture. We have also shown that the distribution function (17) presents a physically correct way to describe quantum chaos. The value of ω is connected with the localization properties of the wave functions. The key variable, however, is the parameter q, which quantitatively describes the chaotic fraction of the phase space in the sense of [47], even for cases far from the semiclassical approximation.

ACKNOWLEDGMENTS

Discussions with A. Bjeliš, V. Dananić, and M. Robnik are gratefully acknowledged.

[1] S. Blumberg and G. E. Porter, Phys. Rev. **110**, 786 (1958).
[2] M. V. Berry and M. Tabor, Proc. R. Soc. London, Ser. A **356**, 375 (1977).
[3] S. W. McDonald and A. N. Kaufman, Phys. Rev. Lett. **42**, 1189 (1979).
[4] G. Casati, F. Valz-Gris, and I. Guarnero, Lett. Nuovo Cimento **28**, 279 (1980).
[5] O. Bohigas, M. J. Giannoni, and C. Schmit, Phys. Rev. Lett. **52**, 1 (1984).
[6] C. H. Lewenkopf, Phys. Rev. A **42**, 2431 (1990).

[7] V. Paar, D. Vorkapić, and A. E. L. Dieperink, Phys. Rev. Lett. **69**, 2184 (1992).
[8] T. Shigehara, N. Yoshinaga, T. Cheon, and T. Mizusaki, Phys. Rev. E **47**, R3822 (1993).
[9] G. Date, S. R. Jain, and M. V. N. Murthy, Phys. Rev. E, 198 (1995).
[10] J. Zakrzewski, K. Dupret, and D. Delande, Phys. Rev. Lett. **74**, 522 (1995).
[11] F. Leyvraz, C. Schmit, and T. H. Seligman, J. Phys. A **29**, L575 (1996).
[12] M. Berry, *Semiclassical Mechanics of Regular and Irregular Motion, Les Houches, 1981* (North-Holland, Amsterdam, 1983), pp. 173–271.
[13] O. Bohigas and M. J. Giannoni, in *Mathematical and Computational Methods in Nuclear Physics*, edited by J. L. Dehesa, J. M. G. Gomez, and A. Polls, Lecture Notes in Physics Vol. 209 (Springer, Berlin, 1984), pp. 1–99.
[14] A. Hönig and D. Wintgen, Phys. Rev. A **39**, 5642 (1989).
[15] F. M. Izrailev, J. Phys. A **22**, 865 (1989).
[16] A. Y. Abul-Magd and M. H. Simbel, J. Phys. G **24**, 579 (1998).
[17] T. Guhr, A. Müller-Groeling, and H. A. Weidenmüller, Phys. Rep. **299**, 189 (1998).
[18] E. J. Heller and S. Tomsovic, Phys. Today **46**(7), 38 (1993).
[19] K. Zyczkowski, in Proceedings of the IV Symposium in Statistical Physics, Zakopane, 1991, Acta. Phys. Pol. B **23**, 245 (1992).
[20] S. Sridhar and E. J. Heller, Phys. Lett. A **46**, R1728 (1992).
[21] J. Stein and H. J. Stöckmann, Phys. Rev. Lett. **68**, 2867 (1992).
[22] P. A. Chinnery and V. F. Humphrey, Phys. Rev. E **53**, 272 (1996).
[23] H. Alt, H. D. Gräf, H. L. Harney, R. Hofferbert, H. Lengeler, C. Rangacharyulu, A. Richter and P. Schardt, Phys. Rev. E **50**, R1 (1994).
[24] A. D. Stone and H. Bruus, Physica B **189**, 43 (1993).
[25] J. A. Katine, M. A. Eriksson, A. S. Adourian, R. M. Westerwelt, J. D. Edwards, A. Lupusaux, E. J. Heller, R. M. Campman, and A. C. Goshard, Phys. Rev. Lett. **79**, 4806 (1997).
[26] I. Mrkonjić, D. Radić, and V. Lopac (unpublished).
[27] R. Artuso, G. Casati, and I. Guarneri, Phys. Rev. E **51**, R3807 (1995).
[28] A. Bäcker, F. Steiner, and P. Stifter, Phys. Rev. E **52**, 2463 (1995).
[29] H. R. Dullin, P. H. Richter, and A. Wittek, Chaos **6**, 43 (1995).
[30] G. Benettin and J. M. Strelcyn, Phys. Rev. A **17**, 773 (1978).
[31] A. Bäcker and H. R. Dullin, J. Phys. A **30**, 1991 (1997).
[32] M. Robnik, Prog. Theor. Phys. Suppl. **116**, 331 (1994).
[33] T. Prosen and M. Robnik, J. Phys. A **26**, 2371 (1993).
[34] M. Robnik, J. Phys. Soc. Jpn. **63**, 131 (1994).
[35] M. Robnik, J. Phys. A **16**, 3971 (1983).
[36] A. Shudo and Y. Shimizu, Phys. Rev. E **47**, 54 (1993).
[37] H. Ch. Schachner and G. H. Obermair, Z. Phys. B **95**, 113 (1994).
[38] P. Bellomo, Pramana, J. Phys. **44**, 85 (1995).
[39] T. Szeredi and D. A. Goodins, Phys. Rev. E **48**, 3529 (1993).
[40] A. Hayli, J. Stat. Phys. **83**, 71 (1996).
[41] A. Bäcker, R. Schubert, and P. Stifter, J. Phys. A **30**, 6873-6795 (1997).
[42] A. Shudo, Phys. Rev. E **47**, 54 (1992).
[43] A. G. Miltenberg and Th. W. Ruijgrok, Physica A **210**, 476 (1994).
[44] R. J. Ridell, Jr., J. Comput. Phys. **31**, 21 (1979); **31**, 42 (1979).
[45] J. B. French and S. S. M. Wong, Phys. Lett. B **35**, 5 (1971).
[46] T. A. Brody, Lett. Nuovo Cimento **7**, 482 (1973).
[47] M. V. Berry and M. Robnik, J. Phys. A **17**, 2413 (1984).
[48] V. Lopac, *Contributions to the 1st Congress of Mathematicians, Physicists and Astronomers of Slovenia, Ljubljana, Slovenia* (Društvo matematikov, fizikov in astronomov Llovenije, Ljubljiana, 1994), p. 82; *Contributions to the European Research Conference on Nuclear Physics: Chaotic Phenomena in Nuclear Physics, Aghia Pelaghia, Crete, Greece*, edited by L. Åberg (European Science Foundation, Lund, 1996), p. 37.
[49] V. Lopac, S. Brant, and V. Paar, Z. Phys. A **356**, 113 (1996).
[50] T. Prosen and M. Robnik, J. Phys. A **27**, 8059 (1994).
[51] T. Prosen and M. Robnik, J. Phys. A **30**, 8787 (1997).
[52] G. M. Zaslavsky, M. Edelman, and B. A. Nyazov, Chaos **7**, 159 (1996).